行政院國家科學委員會專題研究計畫 成果報告

塑膠光子晶體光纖氣體感測器之製作
研究成果報告(精簡版)

計 畫 類 別 ：個別型
計 畫 編 號 ：NSC 97-2221-E-216-012-
執 行 期 間 ：97 年 08 月 01 日至 98 年 07 月 31 日
執 行 單 位 ：中華大學機械與航太工程研究所

計 畫 主 持 人：簡錫新
共 同 主 持 人：馬廣仁

報 告 附 件 ：出席國際會議研究心得報告及發表論文

公 開 資 訊 ：本計畫涉及專利或其他智慧財產權，1 年後可公開查詢

中 華 民 國 98 年 10 月 26 日

行政院國家科學委員會補助專題研究計畫成果報告

※※※※※※※※※※※※※※※※※※※※※※※※

塑膠光子晶體光纖氣體感測器之製作

※※※※※※※※※※※※※※※※※※※※※※※※

計畫類別：■個別型計畫　　□整合型計畫

計畫編號：NSC 97-2221-E -216-012-

執行期間：　97 年　08　月　01　日至　98　年　08　月　31　日

計畫主持人：簡錫新

共同主持人：馬廣仁

計畫參與人員：黃立廷、錢東佑、洪柏嵐

本成果報告包括以下應繳交之附件：

□赴國外出差或研習心得報告一份

□赴大陸地區出差或研習心得報告一份

■出席國際學術會議心得報告及發表之論文各一份

□國際合作研究計畫國外研究報告書一份

執行單位：中華大學

中　華　民　國　98　年　10　月　20　日

行政院國家科學委員會專題研究計畫成果報告

塑膠光子晶體光纖氣體感測器之製作

Fabrication of Photonic crystal fiber based gas sensors

計畫編號：NSC **97-2221-E -216-012**
執行期限：97 年 08 月 01 日至 98 年 07 月 31 日

主持人：簡錫新　中華大學機械系
共同主持人：馬廣仁　中華大學機械系
計畫參與人員：黃立廷、錢東佑、洪柏嵐　中華大學機械系

一、中文摘要

本研究以堆疊及抽拉法製作出塑膠光子晶體光纖(或微結構光纖)，並探討其空孔結構對氣體擴散及對光纖傳輸損失之影響。結果顯示，空孔率大的光纖較有利氣體吸附，對光強度變化影響較大，有利於進行氣體感測。實驗結果顯示氧氣和乙炔可在短時間內吸附再光纖孔壁上達到飽和狀態。乙炔較易吸附在塑膠微結構光纖上，因此量測到傳輸損失比其他氣體高。

關鍵詞：氣體感測、塑膠微結構光纖、能量損失

Abstract

The polymer-based photonic crystal optical fibers (or polymer microsctrucured optical fibers, PMOFs) were fabricated by stack and draw process. The influence of holes structure on the gas diffusion and transmission loss of PMOFs was discussed. The result shows the PMOFs with a higher fraction of holes structure favors more gases to be absorbed, and hence enhanced the transmission loss of PMOFs. The adsorption of O_2 and C_2H_2 gases on PMOFs is faster to achieve saturation state compared to that of N_2 gas. The measured gas adsorption induced transmission loss of polymer PMOFs is greater for C_2H_2 than that of other gases.

Keywords: gas sensing, polymer microstructured optical fiber, energy loss.

二、緣由與目的

光纖感測器是 20 世紀發展出的一種新技術，它可以廣用於氣體、化學及生醫等感測領域 [1]。高分子光纖、多組成份玻璃光纖和熔石英光纖都可用於光纖感測器上。近年來高分子光纖不斷的發展和創新，能量損失也可低於傳統光纖，因此高分子光纖將可取代傳統光纖應用於光纖感測器上 [2,3]。

傳統石英光纖，雖然可以達到能量損失極低的好處，但由於彎曲、耦合不易，造成能量損失等問題未能有效的改善，使其效率明顯降低。應用於氣體感測器上，最大困境在於光的模場與氣體作用區域太小，導致吸收力太差，影響感測訊號的強度，因此需要較長的光纖感測區段來進行感測。但因其製作過程易損傷光纖，製程穩定性不佳，使其產品在未來發展受到限制。相對地，以聚合物材料為主的光纖，有體積小、重量輕、成本低、易彎曲及製程穩定性佳等優點，但對於能量損失較大的問題仍未能解決[4]。

近年來 Eijkelenborg 等人[5,6]利用高分子聚合 PMMA（聚甲基丙烯酸甲酯)成功製造出塑膠微結構光纖，大大降低塑膠光纖的能量損失。塑膠光子晶體光纖具有微結構的特性，提高了光纖氣體感測器的靈敏度，其最大的優勢在於多孔結構提供了感測的區域，微小的光強度變化即可獲得實驗結果。而塑膠微結構光纖的包層亦無需特別處理，可顯著改善傳統光纖感測器製程的穩定性。

三、　實驗方法

本實驗規劃成：抽製實驗用微結構光纖，裁切 PMMA 毛細管成所需要長度 15 cm，

如圖 1(a)，利用超音波洗淨機震洗去除管內的雜質，將數支毛細管堆疊成正六角週期性結構，且將正中央毛細管替換為尺寸相同的實心 PMMA 圓棒，如圖 1 (b)，並在預形體外層加以適當的緊束，以防止升溫燒結過程中，因受熱膨脹而產生的變形，將預形體放入 Lindberg/Blue M 的燒結爐，升溫至 110℃並持溫 3 hr 去除水氣，之後再升溫至 140℃並持溫 2 hr 進行擴散燒結。將燒結完成的預形體放置管型加熱爐內，並且施以適當荷重抽製初步預形體，如圖 1(c)，將抽製完成的預形體再裁切一段約 15 cm，放入抽絲用的管型加熱爐中，進行二次抽製，如圖 1 (d)。

將微結構光纖放入真空腔體中加以固定，以半導體紅光雷射當作光源，利用透鏡將波長為 650 nm 的雷射光聚焦耦合於微結構光纖端面中，在通入待測氣體數分鐘，並以光功率計量測氣體吸附於微結構光纖上光強度變化。實驗中為了避免裁切過程中造成微結構光纖端面的不平整，所造成的光功率損失，因此本實驗將量測完的光纖再裁切一次後進行第二次測量，重複三次實驗取測量值的平均值。

本實驗利用光源為波長為 650 nm，功率為 3.1 Mw 的半導體雷射光源。型號為 EE01AT 的光纖耦合器，並加裝在三軸移動平台上，所使用透鏡為 10 倍。光纖感測器氣體室，為長度 100 mm，兩邊圓管直徑為 10 mm，上下圓管直徑皆為 7 mm 的玻璃管。以型號 TQ8210 的光功率計，作為光能量強度變化的測量。

(a) 裁切

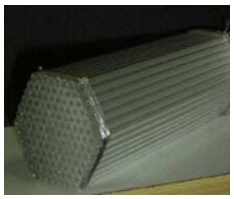

(b) 堆疊和緊束

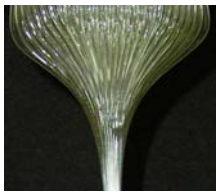

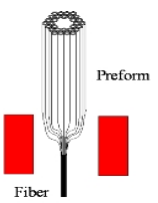

(c)升溫燒結並抽製預形體　(d) 抽絲

圖 1 光纖製作流程;以(a)~(d)的順序製作。

四、結果與討論

4.1 空孔率對氣體感測器靈敏度之影響

由於預形體在溫度 175℃，施以不同的抽制速度會造成不同空孔率的微結構光纖，因此，本研究以抽制速度 5 cm/min，15 cm/min，25 cm/min 進行抽絲。將抽絲完成的微結構光纖以 SEM 檢查微結構是否完整 。將完整的微結構光纖分別取用空孔率 0.47 和 0.52 和 0.59，如圖 2 中(a)、(b)、(c)所示，來進行氣體吸附感測。實驗中，為了避免有誤差，所以選定光纖外徑約為 200-300 μm。

圖 3 中，空孔率為 0.47 的光纖，剛開始的能量損失變化較小，在氣體通入 6 min 後其能量變化明顯平穩許多。而空孔率 0.59 的光纖，再一開始造成能量損失變化幅度較大，與氣體吸附後相互作用明顯增加，因此空孔率大的光纖可以提供較大的作用面積與吸附的氣體相互作用，以提高較大的環境供氣體吸附，而空孔率小的光纖，由於提供的作用面積較小，因此等氣體完全吸附後，其造成的能量損失變化將趨近平穩，由於量測的功率值是以單點時間紀錄一次，因此平穩後微小的變化會對該點量測出的功率值造成微小變化，導致平穩後必非呈現平穩的直線狀。

表 1.1 為不同空孔率的微結構光纖，其中 Core 直徑(D)為纖蕊直徑，孔洞大小(d)為單一纖殼孔洞的直徑，孔洞間距(Λ)為兩個纖殼孔洞中心點的距離，空孔率(d/Λ)則是孔洞大小與孔洞間距的比值。

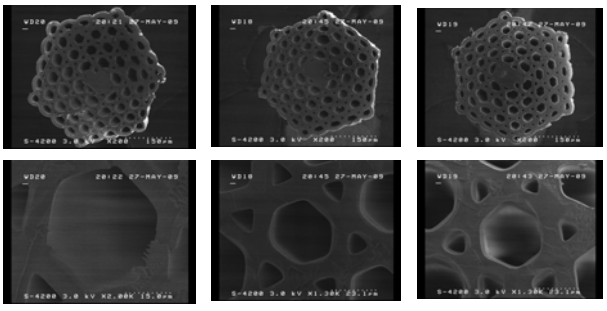

(a) 0.47　(b) 0.52　(c) 0.59

圖 2 塑膠實心蕊微結構光纖顯微組織圖：(a)、(b)、(c)為不同空孔率的結構狀態。

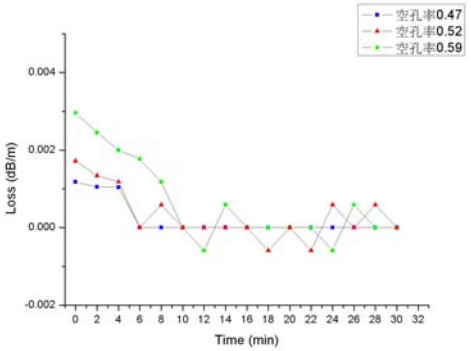

圖 3 不同空孔率的能量損失變化。

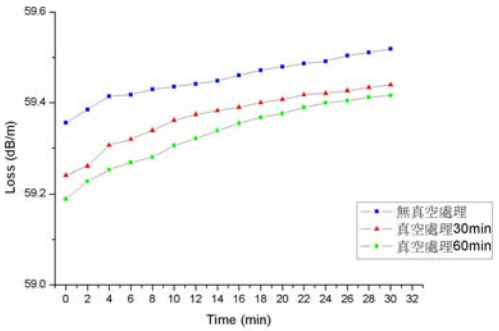

圖 4 無真空處理和真空處理能量損失變化。

表 1.1 抽製速度對微結構光纖空孔率及能量傳輸損失之影響

抽製速度 (cm/min)	Core 直徑 D (μm)	孔洞大小 D (μm)	孔洞間距 Λ (μm)	空孔率 (d/Λ)	Loss (dB/m)
5	64.28	26.16	54.81	0.47	99.35
15	66.86	29.99	53.57	0.52	84.26
25	68.57	34.29	57.71	0.59	61.98

4.2 真空處理對感測器靈敏度之影響

由於光纖原先空孔內的水氣再放入中空腔體中進行氣體感測，實驗中可能會有雜訊產生而影響實驗結果。因此本研究將對光纖抽真空以去除原先空孔內的水氣，以無真空，真空處理 30 min，真空處理 60 min 三種參數，進行氣體吸附的感測實驗，比較不同的真空度處理時間造成的光強度變化，經由真空處理 60 min 其真空度可達到 22 cm/Hg。使用的微結構光纖能量損失約為 59.35 dB/m 左右。

圖 4 中，可以看到未抽真空的光纖，再通入氣體進行感測時，能量損失變化幅度明顯不大，然而隨著抽真空的時間增加，在實驗前光纖量測能量損失時有明顯降低，而且氣體吸附後所造成的能量損失變化幅度較大。所以，抽真空以去除光纖原先空孔內的水氣，可以讓氣體吸附的效果越好，有助於進行氣體感測。

4.3 不同氣體感測結果

當光纖通過介質時，即使不發生反射、折射的現象，其傳播情況也會發生變化。如果光源光譜覆蓋一個或多個氣體分子吸收，當光通過氣體時就會發生衰減，所以可用比爾-郎伯定律(Beer-Lambert Law)來進行分析。波長為 λ 單色光，輸出光強度為 I、輸入光強度為 I_0 與氣體分子之關係為

$$\frac{I}{I_0} = \exp(-\alpha CL)$$

式中 C 為氣體吸收濃度(mol dm^{-3})，α 為單位長度、單位濃度的吸收係數($m^2 mol^{-1}$)，L 為光纖長度(cm)，將上式改寫為下式

$$C = \frac{1}{\alpha L}\ln(I_0/I)$$

當光纖感測器氣體室無待測氣體時，透過氣體室將由功率計量測出的光強度為 I_0，當待測氣體通入氣體室時到達一到濃度 C 時，此氣體對光源發出的光有最強的吸收，所量測出的光強度為 I。於是見由 I_0 與 I 的相比，並有一定程度的衰減產生，通過測得 I_0 與 I 的比值，便可檢測出氣體濃度。

本研究在未通入待測氣體前，將光纖感測氣體室抽氣 60 min，以去除原先光纖空孔的水分和氣體室本身的其他雜質，使其內部腔體處於真空狀態再進行氣體感測實驗。將光纖氣體感測器真空處理後，再通入待測氣體(氮氣、氧氣、乙炔)持續 30 min，以每 2 min 的間隔量測氣體擴散所造成光強度變化。

當通入氮氣後，能量損失有明顯提

高。這是由於氣體吸附於光纖後，氣體本身對光有吸收特性，因而造成一部分光散失。隨著通入氮氣的時間越久，能量損失也逐漸變大。通入氮氣時間在 30 min 後，發現其能量損失未能趨近於平穩狀態，推論其主要原因可能是本實驗室所使用的光源是半導體紅光雷射，而氮氣是惰性氣體而對光的吸收波長並不是近紅外線的原因，所以氮氣對紅外光線的吸收效果較差，較不易吸附在光纖孔壁上，因不易達到飽和狀態。

當通入氧氣時其能量損失有明顯變化，變化範圍約在通入氧氣後至 10 min 間，10 min 後其氣體以完全吸附於光纖表面上了，因此能量損失變化趨近於平穩的狀態且變化幅度將慢慢的緩和下來。由於氧氣對光的吸收波長為 0.761 μm，與近紅外線光波長相近，因此對紅光的吸收效果佳，影響的能量損失變化也較為明顯。經由比爾-郎伯定律(Beer-Lambert Law)公式算出通入氧氣 10 min 後其濃度為 0.0042 mol dm^{-3}。

當通入乙炔造成的能量損失變化明顯增大，其變化趨勢由通入乙炔後到通入時間 12 min 後，在 12 min 過後能量損失變化達近乎平穩的狀態，因為乙炔對光的吸收波長是近紅外線光波長約為 1.53 μm，對本實驗所使用光源半導體紅光雷射其吸收效果佳因此對待測氣體乙炔可短時間吸附於光纖孔壁上達到飽和狀態。經由比爾-郎伯定律(Beer-Lambert Law)公式算出通入乙炔 10 min 後其濃度為 0.0085 mol dm^{-3}。

圖 5 顯示出當通以不同待測氣體，因為擴散速度的不同，所以造成的的能量變化也有所不同。由格銳目擴散定律得知，其分子量越小者，其擴散速率越快。氮氣(N_2)的分子量為 28，乙炔(C_2H_2)的分子量為 30，而氧氣(O_2)的分子量為 32，因此從圖中，可以看出當通以不同待測氣體時，分子量的不同影響在光纖當中的擴散速率，與吸附於光纖表面的速度差異，造成能量損失的變化。以氮氣來說，通入於氣體感測器時，由於分子量較小的緣故，所以擴散速率也越快，造成能量變化幅度大，但其最終未達到平穩狀態，所以氣體感測靈敏度較低，而氧氣和乙炔這兩種待測氣體，分別於通入氣體 10 和 12 min 後其能量損失變化便可以達到平穩狀態。

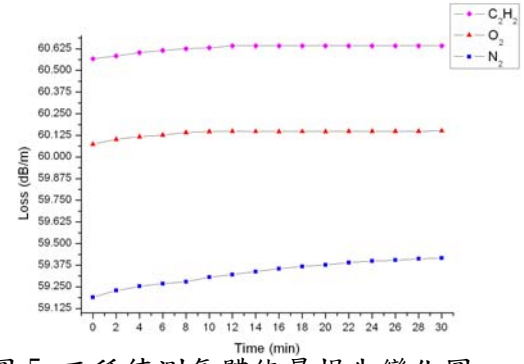

圖 5 三種待測氣體能量損失變化圖

五、結論

1. 由實驗中可發現不同空孔率大小的光纖可提供不同的氣體吸附環境，空孔率大的光纖，可以提供的較大的面積與氣體相互作用，可以增加光強度訊號的變化。空孔率小的光纖，由於本身纖殼的孔徑較小，因此氣體能吸附的面積也較小，氣體吸附於光纖後對光強度訊號變化較小。
2. 研究中可以發現先將氣體感測室抽以真空狀態，能有效降低光纖原先空孔吸附的水氣，可以減少氣體感測時的雜訊，已提高實驗的準確性。
3. 氮氣吸附於光纖後造成光傳輸強度發生明顯的變化，但經 12 min 過後仍未達到穩定狀態，其原因可能是氮氣為惰性氣體，較不易吸附在光纖孔壁上，因此較不易達吸附飽和狀態。氧氣和乙炔可在短時間內吸附再光纖孔壁上達到飽和狀態。乙炔較易吸附在塑膠光子晶體光纖上，因此量測到傳輸損失比其他氣體高。

六、參考文獻

1. C. Elosua, I. R. Matias, C. Bariain and F. J. Arregui, “Volatile Organic Compound Optical Fiber Sensors: A Review”, Sensors, 1440-1465, June, 2006.
2. J. Zubia and J. Arrue, “Plastic Optical Fibers: An Introduction to Their Technological Processes and Applications”, Optical Fiber Technology 7, pp.101-140, 2001.

3. B. V. Chernyak and J. Maryles, “Bio-Chemical Sensor Based on Imperfected Plastic Optical Fiber”, Proceeding of SPIE, Vol. 6585, 65851V, 2007.
4. P. Polishuk, “Plastic Optical Fibers Branch Out”, Communications Magazine, Vol. 247, pp.140-148, 2006.
5. M. A. van Eijkelenborg, M. C. J. Large, A. Argyros, J. Zagari, S. Manos, N. A. Issa, I. Bassett, S. Fleming, R. C. McPhedran , C. M. de Sterke and N. A. P. Nicorovici, “Microstructured Polymer Optical Fibre”, Optics Express, Vol. 9, No. 7, pp.319-327, 2001.
6. M. A. van Eijkelenborg , A. Argyros, G. Barton, I. Bassett, F. Cox, M. Fellew, S. Fleming, G. Henry, N. Issa, M. Large, S. Manos, L. Poladian, J. Zagari, “New Possibilities with Micro-structured Polymer Optical Fiber”, 2002

中華大學補助教師出席國際性及大陸地區海峽兩岸學術會議報告

98 年 07 月 20 日

報告人姓名	馬廣仁	系所 職稱	機械系 副教授
會議時間地點	義大利羅馬	本校核定 補助字號	中華民國 98 年 06 月 15 日 (98)中華研國字第 54 號
會議 名稱	(英文) 5th International Conference on Diffusion in Solids and Liquids (DSL 2009)		
發表 論文 題目	(英文) 1. **The Effect of TaN Interlayer on the Performance of Pt-Ir Protective Coatings in Glass Molding Process** **2. Thermal Stability of Al_2O_3 Coated Low Transition Temperature Glass**		

報告內容應包括下列各項：

一、參加會議經過

第一天：REGISTRATION、AUDITORIUM、POSTER SESSION

第二天：PARALLEL SESSIONS、GALA DINNER BUFFET

第三天：PARALLEL SESSIONS、CITY TOUR

<table>
<tr><td> 
</td><td>  </td></tr>
<tr><td>研討會開幕式</td><td>研討會會場</td></tr>
</table>

二、與會心得

此研討會屬於大型之研討會，使我對於其他國家在相關領域的研究成果有初步了解，也經由聽取其他與會者的報告而拓展了我的思維，相信對我在此研究領域後續的研究上有相當大的助益。在此研討會也可見到許多來自不同國家的學者的研究方式差異，也因此提供了不少的研究方向。

本投稿之文章屬於材料性質之文章，於研討會中見到許多學者對於模擬數學上有許多構思，也因為許多其他投稿文章內容解決了一些研究上無法解決的事情。

三、考察參觀活動(無是項活動者省略)

參觀梵蒂岡博物館以及羅馬競技場

四、建議

無

五、攜回資料名稱及內容

1. 研討會參考資料一份
2. 研討會論文光碟一份

六、其他

無

Thermal Stability of Al_2O_3 Coated Low Transition Temperature Glass

K.J. Ma[1,a], H.H. Chien[1,b], SV P. Vattikuti [1,c], C.H. Kuo[1,d], Z.B. Huo[2,e] and C.L. Chao[2,f]

[1]Institute of Engineering Science, Chung Hua University, No. 707, Sec. 2, Wu Fu Rd., Hsin Chu, Taiwan 30067.

[2]Department of Mechanical and Electro-Mechanical Engineering, Tam-Kang University, No.151 Ying-Chuan Road, Tamsui, Taipei Hsien, Taiwan 251.

[a]ma600229@ms17.hinet.net, [b]hhchien@chu.edu.tw, [c]prabhakar surya vsv_sun@yahoo.com
[d]pots0382@yahoo.com.tw, [e]694341594@s94.tku.edu.tw, [f]clchao@mail.tku.edu.tw

Keywords: sol-gel coating, Al_2O_3, thermal stability, glass molding

Abstract. There are growing varieties of glasses available on the market for the manufacture of molded optical lenses. The glass with low transition temperature (Tg) has the advantage of extending the service life of molding dies. However, most of low Tg glasses have high content of alkali metal oxides and tend to induce severe glass sticking problems. This has made the molding process of these kinds of glasses very difficult indeed. The low Tg glasses normally demonstrate poor chemical durability and scratch resistance. As a result, the yields of fabricating the glass-preforms are frequently rather low. This research tried depositing very thin layer of aluminum oxide on various glass-preforms by water based sol-gel process. High temperature glass wetting experiment was carried out to investigate the high temperature interfacial reaction between the coated glass gobs and stainless steel substrate.

It was found that, when the uncoated glass-preforms were brought in contacted with stainless steel, the contact angle decreased with increasing heating temperature and duration. Owing to the severe interfacial chemical reaction, the originally transparent glass was gradually turned translucent. In the case of Al_2O_3 coated glass-preforms, the variation of the contact angles were very limited, which presented no sticking and no wetting behavior. There was no reaction products could be detected on the contact area after wetting test. The optical transmission of those lenses molded from the coated glass-preforms exhibited no or very little changes after the molding process.

Introduction

The glass molding process is considered to have a great potential for the mass production of aspherical and free form glass lenses with high precision and lower cost [1, 2]. In glass molding process, the die surfaces are exposed to the chemically active glass and also subjected to mechanical and thermal cyclic operations, which leads to three critical problems including sticking/adhesion of glass to the die surface, oxidation and wear of the die. These problems result in imperfections in the glass products, loss of dimensional control of glass products and limited service life of dies. To develop protective coating on the mold surafce and low transition temperature (Tg) moldable glasses are the most popular approaches to improve above mensioned problems.

The precious metal alloys and amorphous carbon based coatings have been widely used as protective coatings to improve glass contact induced sticking problems [3-5]. The thickness and

chemical composition of coatings need to be optimized to achieve satisfied protecting effects. However, protective coating on the mold is unable to avoid volative or unstable elements evapoarted from glass and redeposited on the mold surface.

The glass with low transition temperature (Tg) has the advantage of extending the service life of molding dies because the molding temperature is significantly reduced [6, 7]. However, most of low Tg glasses have high content of alkali metal oxides and tend to be decomposed at high temperature and may induce severe glass sticking problems [8]. Furthermore, The low Tg glasses normally demonstrate poor chemical durability and scratch resistance. As a result, the yields of fabricating the glass-preforms are frequently rather low. These issues have made the molding process of these kinds of low Tg glasses very difficult indeed.

Recently, some researches proposed to apply a very thin carbon or carbon-hydrogen based coating on glass performs to suppress the unstable elements diffusion and hence improve glass sticking problems [9]. However, some drawbacks still existed for these coatings: (1) thermal decomposed C: H coatings with hydrogen trapped in the film may result in the reduction of oxide glass. (b) the a-C or C: H film is unstable at high temperature. Both effects may cause glass sticking on the mold.

It is expectable to apply a more stable oxide layer on glass performs to avoid glass sticking with the molds. Al_2O_3 is one of the candidate coatings due to its high chemical and thermal stability. It also can be applied on the glass preforms with good surface coverage by sol-gel process. Typically, colloidal sol-gel ceramic process is classified according to the precursors used in, including water-based processes that start from a solution of metal salt and alcohol-based processes that derive from a metal alkoxides. In comparison, the water-based sol-gel process can provide the following advantages over alcohol-based process: (1) better surface coverage and thickness uniformity (2) water base films without organic residues and stable at high temperature (3) low temperature process.

This research tried depositing very thin layer of aluminum oxide on L-BAL42 glass preforms by water based sol-gel process. High temperature glass wetting experiment was carried out to investigate the high temperature interfacial reaction between the coated glass gobs and stainless steel substrate.

Experimental

50 mol of alumina acetate dihydrate was mixed with 100 mL diluted water, and then concentrated solution was continuously stirred at 25°C for 2h. The diluted water act as solvent for solution. Gelation and condensation of the derive solution through suitable method. The PH value of water based Al_2O_3 sol-gel coating is approximately 4~4.1. Mirror-polished Grade 304 stainless steel plates with dimensions 15mm x 15mm x 1 mm and glass balls (Ohara L-BAL 42) with 6 mm diameter were choice as substrates and glass preforms. The composition of the glass ball is shown in Table 1. All glass preforms were dipped into solution bath for 30 seconds, and then withdrawn at a speed of 5 ~200 cm/min and to be dried in air for 2 minutes inside the clean room. Finally, the coated glass preforms were placed into a vacuum furnace to carry out annealing treatment at 530°C for 30 minutes. The thickness of Al_2O_3 film can be controlled by the drawing speed in dip coating process.

High temperature glass wetting experiment was carried out in N_2 ambient to investigate the high temperature interfacial reaction between the coated glass gobs and stainless steel substrate, as

shown in Fig.1. Glass wetting images can be in-situ taken using a CCD camera and image analysis was performed with a computer. The morphology, reaction products and crystal structure were investigated by optical microscope (OM), high resolution electron scanning microscope (HRSEM), EDX and XRD. Molding glass optical lenses were carried out by Toshiba press molding machine at a molding temperature of 580℃ to examine the plastic extension behaviour of Al_2O_3 film.

Table 1 Composition of Ohara L-BAL 42 glass

Content	SiO_2	BaO	B_2O_3	Al_2O_3	ZnO	Sb_2O_3
Composition in Wt. %	40-50	20-30	2-10	2-10	2-10	0-2

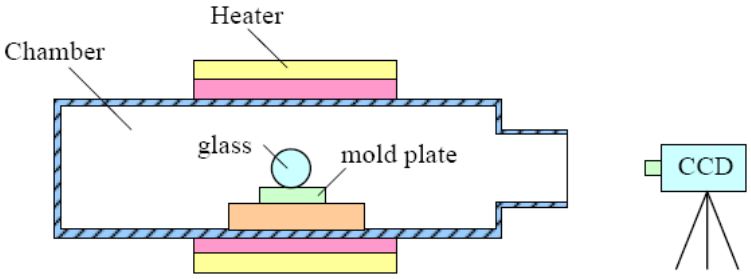

Fig. 1 Schematic drawing of experimental set up for the measurement of high temperature wetting angle

Results and discussions

Hydrolysis and polycondensation reactions of the alkoxy and hydroxyl group take place during the deposition and drying stages at the room temperature. The cross-sectional SEM image shows Al_2O_3 film with smooth and dense structure, as shown in Figure 2. The measured thickness of Al_2O_3 film is 34 nm at a drawing speed of 200 mm/min and the variation of film thickness is less than 10 %. The XRD results present amorphous structure after annealed treatment.

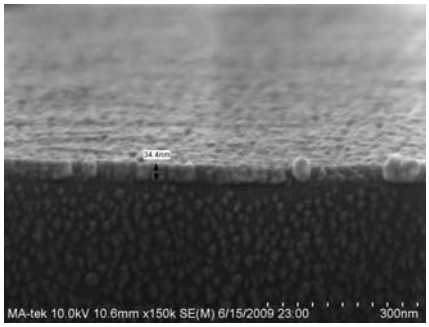

Fig. 2 Cross-sectional SEM image of sol-gel Al_2O_3 coated glass ball after annealing treatment

The pictures of glass balls recorded at 825°C after 5 minutes holding period are shown in Fig. 3(a). In the case of uncoated glass ball, the contact angle was decreased from 155° to 32° at 825°C. However, the Al_2O_3 coated glass still remained high contact angle (136°) when contacted with stainless steel substrate (Fig. 3(b)).

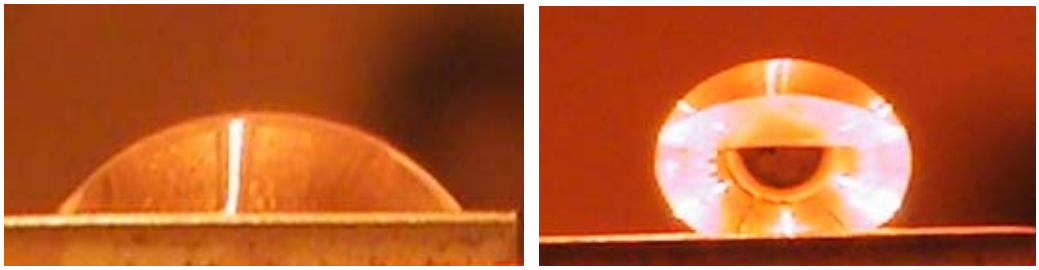

(a)

(b)

Fig. 3 Images of the contact angle of (a) uncoated glass ball and (b) Al_2O_3 coated glass ball on the stainless steel at 825°C after holding 5 minutes

The variation of the contact angle with respect to the temperature profile from 550 to 825℃ and processing time is shown in Fig. 3. The result can be classified into 3 stages, such as heating, holding and cooling stages. In the first stage, the contact angles of molten glass slowly decrease from 550 to 825℃ followed by a very slow spreading kinetics for uncoatedglass balls. In the second stage the temperature was kept at 825°C for five minutes. The contact angle was rapidly decreasing with respect to holding period. In the third stage, the contact angles present unobserved changes. The total cycle time is twenty five minutes.

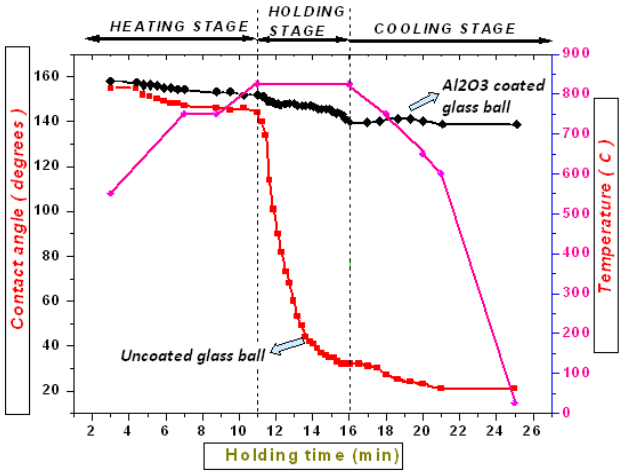

Fig. 3 The variation of contact angle as a function of holding time and temperature for uncoated and sol-gel Al_2O_3 coated glass ball on stainless steel

The interfacial reaction between the substrate and nucoated molten glass has been investigated through EDX analysis and elements mapping (Fig. 4). The results indicate that high affinity reactive elements Cr, Fe, and Ni enhance chemical reactions, resulting in the formation of Cr-O, Fe-O and Ni-O based complex compounds layer at the interface. It has also observed that some of the reactive elements Si and Ba diffused out from the molten glass into the substrate. The obvious mass diffusion and redox reaction occurred at interfaces, which resulted in the decrease of the contact angle. The second possible mechanism to reduce contact angle may be from the surface roughness of the substrates and other physical forces which needs to be further studied.

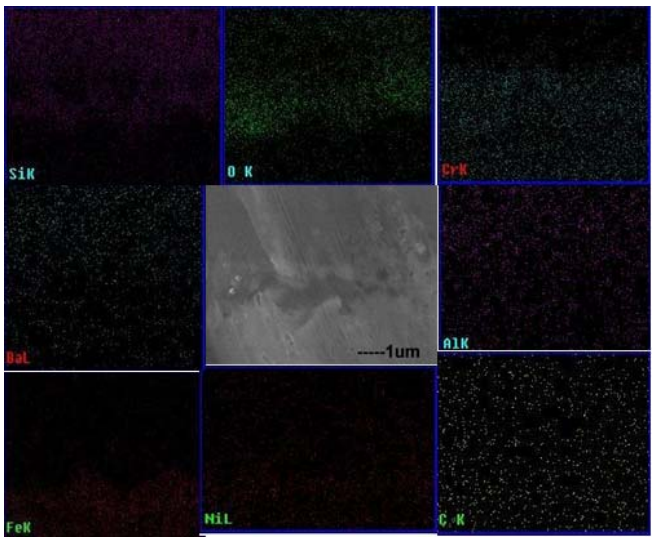

Fig. 4 Cross-sectional view at the interface of the uncoated glass preform/stainless steel substrate with element mapping results

The wetting curve shows very interesting results for Al_2O_3 coated glass ball. The variation of the contact angles varied from 152 to 136° with very little change in contact angle, presents anti-sticking or non-wetting behavior (Fig. 3). The Al_2O_3 coated glass ball still remains fully transparent after wetting test when contacted with stainless steel substrate (Fig. 5(a)). The surface of stainless steel contacted with Al_2O_3 coated glass ball remains smooth and clean (Fig. 5(b)). Although stainless steel was oxidized, there is no observable glass sticking products, such as Zn, Ba, Al and Si oxides to be detected on the glass contacted surface (Fig. 5(c)). It means that there is no detectable chemical interaction occurred at the interfaces between the Al_2O_3 coated glass ball and stainless steel substrate. The sol-gel coated Al_2O_3 film acted as an excellent diffusion barrier which effectively inhibit the element diffusion and reaction between the substrate and glass. This is the reason why the final contact angle of Al_2O_3 coated substrate has little change at 825°C.

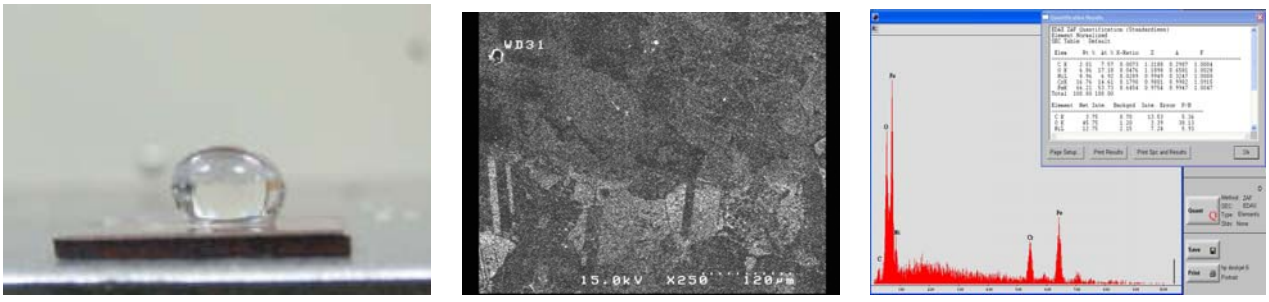

(a) (b) (c)

Fig. 5 (a) Appearance of Al_2O_3 coated glass ball (b) SEM image of stainless steel and (c) EDX results after wetting test

Fig. 6 shows the elements depth profile of Al_2O_3 coated lens after glass molding test at 580℃. It shows that the Al_2O_3 film is thermodynamic stable phase which can effectively hinder out

diffusion of elements such as Si, Zn, B and Ba at 580℃. Carbon based contaminants still exist on the Al_2O_3 coated glass surface which need to be avoided.

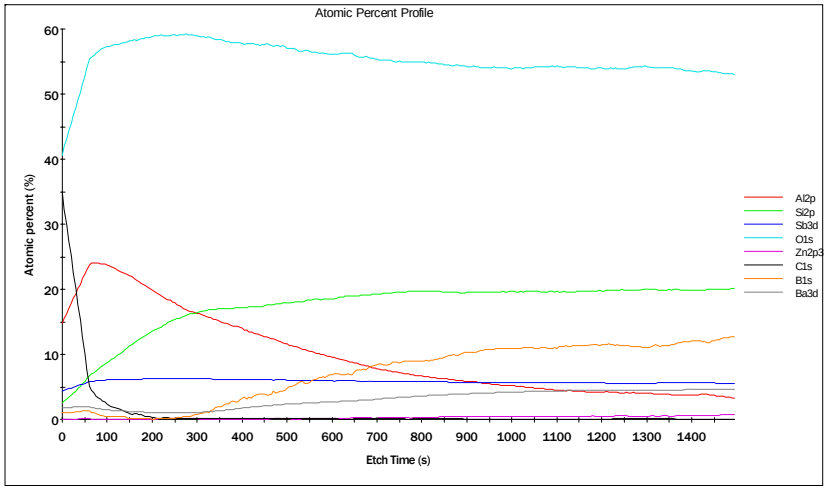

Fig. 6 Elements depth profile of Al_2O_3 coated glass lens produced by molding process at 580℃.

A desired optical lens is obtained by press molding a glass preform using stainless steel material as the mold (Fig. 7(a)). When press molding a glass materials having a Al_2O_3 film on the surface, deformation of the glass materials is accompanied by extension of Al_2O_3 film on the surface. When extension of the Al_2O_3 film cannot keep up with deformation of glass material, breach will occur. Thus, the glass material is exposed at the breached portions, resulting in the risk of fusion to the molding surface. Our results showing the surface of molded lens appear defectless within the designed the aspherical aperture when the thickness of Al_2O_3 film is 34 nm (Fig. 7(b)). The breaches only appear near the edge of the molded lens due to a greater glass deformation on this portion (Fig. 7(c)). The thickness of Al_2O_3 film less than 15 nm is suggested to completely avoid breaches on the whole molded lenses.

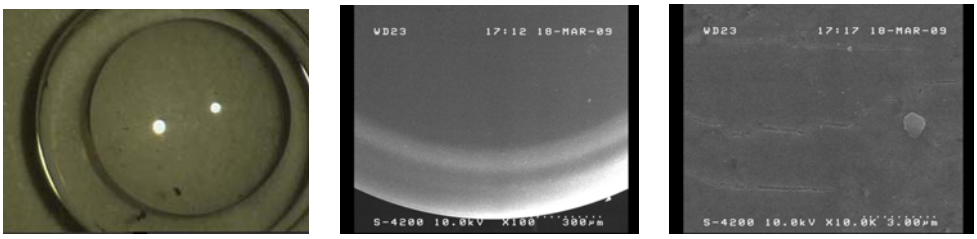

(a) (b)

(c)

Fig. 7 (a) Appearance of molded lens (b) SEM surface image of molded lens and (c) high magnification SEM image near the edge of the molded lens

5. Conclusions

The final contact angles of the uncoated and Al_2O_3 coated glass preform contacted with stainless steel are observed to be 32° and 156° respectively at 825°C for 5 minutes holding period. The Al_2O_3 coated glass preforms demonstrated an excellent anti-sticking behavior compared to that of uncoated ones. The SEM/EDAX analysis shows no detectable interaction between the Al_2O_3 coated

glass and stainless steel substrates. It is believed that applying a stable Al_2O_3 film on glass performs can significantly improve glass sticking problems and hence extend the service life of optical molds.

Acknowledgement

This work was supported by the National Science Council of R.O.C. under contract NSC-96-2211-E-216-030. Glass molding was done at Shining Optics Ltd, Taiwan, R.O.C..

References

[1] H. Torii, M. Aoki, H. Okinaka, S. Yuhaka, S. Yuhaku and S. Nakamura, U.S. Patent 4,606,750. (1986)

[2] M.A. Angle, G.E. Blair and C.C. Maier, U.S. Patent 5,217,516. (1974)

[3] J. Brand, R. Gadow and A. Killinger: Surface and Coatings Technology Vol. 180-181 (2004), P. 213

[4] K. Yamamoto, K. Hirabayashi, N. Kurihara, Y. Taniguchi and K. Ikoma, US Patent 5026415. (1991)

[5] M. Umetani, H. Monji, M. Sunohara, J. Murata, T. Takano, Y. Shirafuzi, Y. Inoue and K. Kuribayashi, U.S. Patent 5,171,348. (1992)

[6] Information on http://www.schott.com

[7] Information on http://www.oharacorp.com

[8] K.J. Ma, H.H. Chien, W.H. Chuan, C.L. Chao and K.C. Hwang: Key Engineering Materials Vols. 364-366 (2008), p. 655

[9] T. Igari and S. Ohmi, US Patent 2004/0261455 A1. (2004)